Ground Segment Architectures for Large LEO Constellations with Feeder Links in EHF-bands

Iñigo del Portillo*, Bruce Cameron, Edward Crawley
Massachusetts Institute of Technology
77 Massachusetts Ave 33-409
Cambridge, MA 02139
{portillo, bcameron, crawley}@mit.edu

***Abstract*—In recent years, several large constellations of LEO satellites have been proposed by different companies as a means to provide global broadband. Even though the first generation of these systems was designed using Ka-band feeder links, the saturation of the Ka-band spectrum, the need for wider bandwidths, and the increasing demand for capacity are driving the industry towards the development of systems with feeder links operating in EHF bands (30 - 300 GHz). The two main advantages of transitioning towards higher frequency bands are: one, the possibility of using the larger bandwidth allocations available for higher capacities, and two, a reduction in the number of ground sites required to support such capacity. However, there are trade-offs that need to be further explored, since links operating at higher frequencies are impaired by higher atmospheric attenuation, which in turn causes outages and might require of additional ground stations to maintain QoS levels (i.e., given coverage and availability requirements).**

This paper compares ground segment architectures for constellations using feeder links in Q/V-band against those using E-band. We develop a method to determine the locations of the minimum number of ground stations that maximize the system capacity while achieving desired QoS levels. To that end, first, we use International Telecommunication Union (ITU) models to characterize the atmospheric attenuation in EHF-bands; next, we describe a Monte Carlo simulation method to estimate the statistics of the data-rate achieved when multiple ground stations are within the line-of-sight (LoS) of a given satellite. Finally, we present the results in terms of the number of ground stations required and data-rates achieved, after optimizing over the different ground station locations for both the Q/V-band and E-band scenarios. We then compare these results to the ones obtained using current systems in Ka-band.

TABLE OF CONTENTS

1. INTRODUCTION

Motivation

To satisfy the higher demand for satellite-delivered global broadband services, multiple companies have proposed in the last two years large constellations of LEO satellites [1], [2], [3], [4]. These space-borne systems aim to offer a service with quality comparable to fiber-based terrestrial systems, and will be used both to provide direct voice and data access to consumers and businesses and as a backhaul network to extend connectivity of mobile operators and ISPs.

Although this new wave of non-geosynchronous orbit (NGSO) constellations share some similarities with early proposals that failed to raise financing in the late 1990s, there have been several breakthroughs in the last two decades that suggest current proposal will not suffer the fate of their predecessors; the advancements in electronics and antenna technology, the spread of advanced modulation and coding (MODCOD) schemes, a larger market for broadband and mobile communications, and considerably lower launch costs, all contribute towards greater viability.

And while most of these new proposals are designed using a "Ku-band user links, Ka-band feeder links" architecture, the saturation of the Ka-band spectrum, the need for wider bandwidths, and the increasing demand for capacity are driving the industry towards the development of systems operating in EHF bands (30 - 300 GHz). In particular, frequency allocations in Q/V-band (37.5-42.5 GHz for space-to-Earth, and 47.2 - 50.2 GHz and 50.4-51.4 GHz for Earth-to-Space) and in E-band (71-76 GHz as space-to-Earth and 81-86 GHz as Earth-to-Space) are being considered as key technologies for high throughput satellites (HTS) [5], [6] and large LEO constellations [7], [8].

Arguments in favor of transitioning to higher frequency bands include the increase in bandwidth available, (which in turn increases system capacity), and a potential reduction in the number of ground sites required. However, the latter advantage bears further discussion, given that links operating at higher frequencies are impaired by higher atmospheric attenuations, which causes link outages and might require additional ground stations to maintain QoS levels (i.e., given coverage and availability requirements).

Several missions in GEO have been using Q-band communications during the last 25 years, even though none of them were commercial satellite communication missions: ITALSAT F1 and F2 [9], and Alphasat [10] were technological demonstration missions, whereas SICRAL 1, MILSTAR [11], and AEHF [12] were fully operational military missions. From a theoretical perspective, Q-band and E-band systems have been extensively analyzed when used as feeders links for commercial geostationary communication satellites [13], [14], and the reductions in costs and increases in capacity have been quantified [15], [16]. Furthermore, previous work has analyzed the optimal site locations for the ground segments of LEO [17] and GEO [18] systems that use optical feeder links, a somehow similar problem since the presence of clouds induces outages in the links and availability considerations are critical. For EHF frequency

978-1-5386-2014-4/18/$31.00 ©2018 IEEE

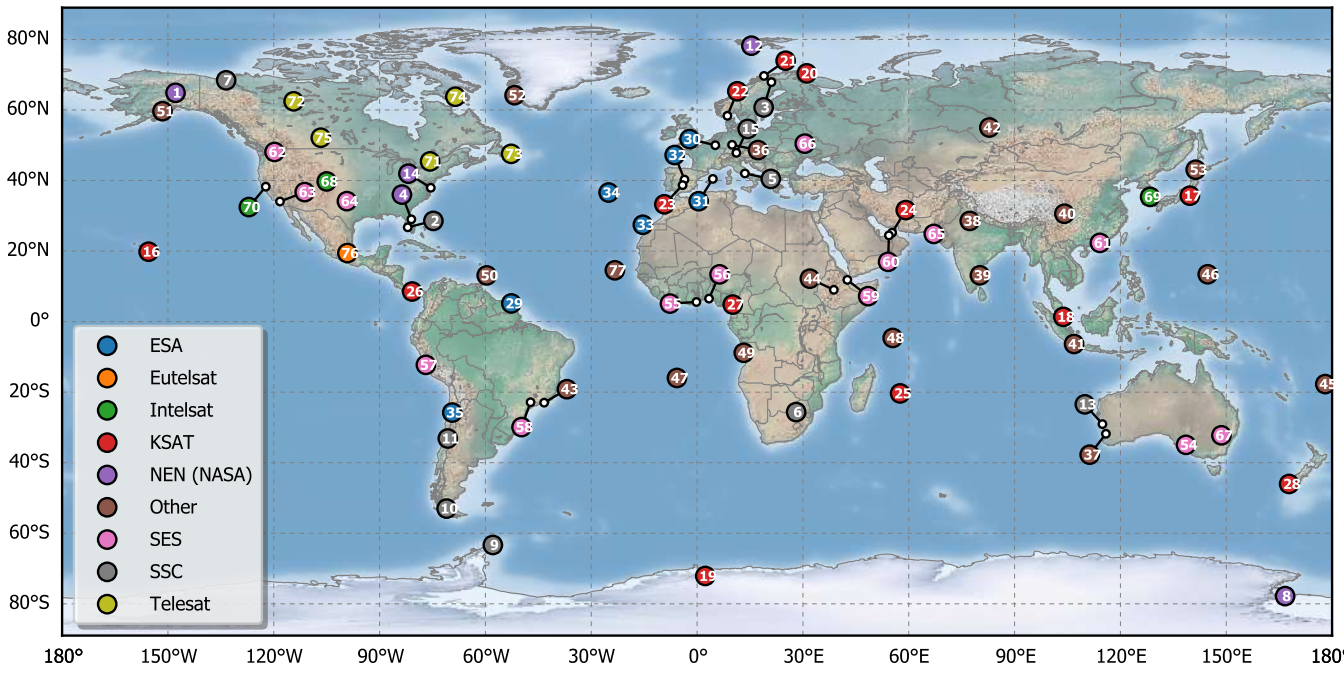

Figure 1: **Candidate ground stations for our analysis. For further details of the exact location of the ground stations check Table 8.**

bands, no analyses have been undertaken to determine the optimal ground station locations and to quantify the impact of using them as feeder links for LEO constellations.

This paper compares ground segment architectures for LEO constellations that use Q/V-band or E-band feeder links against current architectures that use Ka-band. In particular, we describe a method to determine the optimal location of the ground stations that maximize system capacity, while achieving desired QoS levels. To that end, we develop a Monte Carlo simulation method to estimate the joint statistics of the data-rates achieved when multiple ground stations are within the line-of-sight of a given satellite, using ITU models to estimate the atmospheric attenuation in EHF-bands.Results for the optimized ground segments are presented in terms of the number of ground stations vs. data-rates achieved, for the Q/V-band and E-band scenarios. We then compare these results to the ones obtained using current designs in Ka-band.

Paper Organization

The remainder of this paper is organized as follows: Section 2 presents the problem formulation, the assumptions for the space and ground-segment of the scenarios analyzed, and the mathematical statistical model developed to estimate the data-rate achieved. Section 3 describes the models for the link budget, atmospheric attenuation, and demand, together with the optimization algorithms used to determine the optimal location of the ground stations. Section 4 presents the results of our analysis, quantifies the impact of using EHF bands, and compares the performance and cost of EHF-band systems to Ka-band systems. Lastly, Section 5 summarizes our conclusions and outlines future directions of research.

2. Problem Formulation

The primary objective of this paper is to quantify the improvements in terms of data-rate achieved and/or reduction in the number of ground stations that result from using EHF-band feeder links for large LEO constellation. This quantification, however, is subject to assumptions with regard to the topology of the constellations, the locations of the ground stations, and the metrics used to measure quality of service (QoS). This Section presents our assumptions in these areas for the scenarios analyzed.

In addition, because the data-rate achieved is largely dependent on the atmospheric attenuation, a stochastic process in nature, a statistical model is needed to quantify the impact of using EHF-bands. The last part of this Section describes the mathematical model we developed to compute the achievable data-rate when multiple ground stations are within the line-of-sight of the satellite.

Ground station candidate locations considered

To achieve simultaneously the desired data-rate, coverage, and level of redundancy while minimizing cost, it is crucial to optimize the ground segment of a space communications system. We consider that our ground segment is composed of a subset of ground stations out of a set of candidate locations. This candidate set is composed of 77 locations, which were chosen from the ITU Space Network List database [19], attending to the following criteria:

- **Global coverage is guaranteed**: Ground stations are located in all continents since the LEO constellations operate on a global scale. Figure 1 depicts a global map with the location of the candidate ground stations. Broken down by regions, there are 12 candidate stations in Africa, 14 in Asia,

Table 1: **Summary of proposed LEO constellations designs.**

	OneWeb-Ka	OneWeb-V	Boeing - V	SpaceX-Ka	TeleSat - Ka	Telesat - V
FCC filing #	20160428-00041	20170301-00031	20160622-00058	20161115-00118	20161115-00108	20170301-00023
Filing date	4/28/2016	03/01/2017	6/22/2016	11/15/2016	11/15/2016	3/1/2017
# satellites	720	720 + 1280	2956	4425	117	117
# planes	18	34	74	83	11	11
Orbit type	LEO	LEO-MEO	LEO	LEO	LEO	LEO
Orbital info (#plane x #sat alt @ inc)	18x36 1200@87.9°	18x36 1200@87.9° 16x80 8465@45.5°	35x32 1200@45° 18x46 1210@55° 21x48 1000@88°	32x50 1150@53° 32x50 1110@53.8° 8x50 1130@74° 5x75 1275@81° 6x75 1325@70°	6x12 1100@99.5° 5x9 1248@37.4°	6x12 1100@99.5° 5x9 1248@37.4°
ISL	No	No	No	Yes, optical	Yes, optical	Yes, optical
Service band	Ku	V	V	Ku	Ka	V
BW service links	2 GHz	2 GHz	5 GHz	2 GHz	2.1 GHz	4.5 GHz
Service user-sat	12.75 - 13.25 GHz 14.0 - 14.5 GHz	48.2 - 50.2 GHz	47.2 - 50.2 GHz 50.4 - 52.4 GHz	14.0 - 14.5 GHz	27.5 - 29.1 GHz 29.5 - 30.0 GHz	47.2 - 50.2 GHz 50.4 - 51.4 GHz
Service sat-user	10.7 - 12.7 GHz	40.0 - 42.0 GHz	37.5 - 42.5 GHz	10.7 - 12.7 GHz	17.8 - 18.6 GHz 18.8 - 19.3 GHz 19.7 - 20.2 GHz	37.5 - 42.0 GHz
Min el. angle	55	45	45	40	10	?
Feeder band	Ka	V	V	Ka	Ka	V
BW feeder links	2.1 GHz	5 GHz	5GHz	2.1 GHz	2.1 GHz	4 GHz
Feeder sat-GW	17.8 - 18.6 GHz 18.8 - 19.3 GHz 19.7 - 20.2 GHz	37.5 - 42.5 GHz	37.5 - 42.5 GHz	17.8 - 18.6 GHz 18.8 - 19.3 GHz	17.8 - 18.6 GHz 18.8 - 19.3 GHz 19.7 - 20.2 GHz	37.5 - 42.0 GHz
Feeder GW-sat	27.5 - 29.1 GHz 29.5 - 30.0 GHz	42.5 - 43.5 GHz 47.2 - 50.2 GHz 50.4 - 51.4 GHz	47.2 - 50.2 GHz 50.4 - 52.4 GHz	27.5 - 29.1 GHz 29.5 - 30.0 GHz	27.5 - 29.1 GHz 29.5 - 30.0 GHz	47.2 - 50.2 GHz 50.4 - 51.4 GHz
# sim. gateways	1 (2 antennas)	1 (2 antennas)	?	1	2	2
D. GW antenna	2.4 m	1.2 - 3.4 m	?	1 - 3.5 m	3.5	1.8

15 in Europe, 19 in North America, 7 in Oceania, and 10 in South America.

- **Candidate locations do not present strong spatial correlations**: the distance between pairs of ground stations is large enough so that the spatial weather correlation is minimized and therefore weather conditions at earth stations can be considered independent. In particular, in any of the ground segments considered the minimum pairwise distance between ground stations is 2,000 km, which attending to the model provided in recommendation ITU-R P.618-12 [20] (Eq. 1), results in a correlation coefficient below 3%.

$$\rho = 0.59e^{-\frac{|d|}{31}} + 0.41e^{\frac{-|d|}{800}} \quad (1)$$

- **Stations should be realistic potential sites**: All the candidate locations chosen are currently operative teleports, which is part of the ground segment of a large satellite operator.

The complete list with the name, GPS coordinates, and operator of each ground station can be found at the end of this paper in Table 8.

Reference constellation description

We use the large LEO constellation designs proposed by OneWeb, SpaceX, Telesat and Boeing in the last two years to define the reference constellation design for the scenarios analyzed in this paper. Table 1 compares the characteristics of the constellation designs proposed by the four aforementioned companies. Note that most of the designs have planes in the $\sim$ 1,200 km orbital altitude band, as well as a minimum elevation angle for the users' very small aperture terminals (VSAT) of $\sim$ 45 °. Hence, our reference constellation includes a combination of polar and non-polar orbital planes with an orbital altitude of 1,200 km, and the minimum elevation angle for a user VSAT to communicate with a satellite is 45 °. We also assume that the feeder links operating in Ka-band, Q/V-band, or E-band are the limiting factors of the system (i.e., we assume that user links are designed and sized appropriately, and that a frequency reuse scheme has been designed such that all the capacity can be forwarded to the users). Moreover, we assume that satellites have two feeder antennas that can be used simultaneously, and that the gateway dishes have a diameter of 2.4 m.

Inter-satellite links (ISL) play a crucial role when designing the ground segment. If the constellation does not have ISL, each satellite must be in line-of-sight with at least one gateway whenever the satellite is active; if ISL is present, such requirement will not apply. In this study, we consider that there are no inter-satellite links. Finally, note that the total number of planes and and the number of satellites per plane does not have a strong impact in the choice of ground station locations, but affects to the number of dishes on each location.

Metrics

The improvements achieved by using an EHF band for the feeder links of a system need to be assessed by considering different metrics, namely coverage, availability, and data-rates, as well as the number of ground stations required. While the number of ground stations is a proxy for the cost of the system, the other three metrics evaluate its performance, and whether it satisfies QoS requirements.

A critical requirement for all satellite systems is availability, a measure of the percentage of time that the system is operative. A common target value for availability for systems which provide data services using high frequency bands is 99.5%.

In contrast, typical operating conditions are those that are present during **most** of the time. In this paper, we consider typical conditions as those that are present at least, 95% of the time. The system architect specifies requirements in terms of coverage and data-rate for typical conditions and for conditions close to the availability threshold. Note that the performance of the system at the threshold might be considerably degraded compared to typical operations, but still meet the requirements defined by the system architect.

Given these considerations, the two main metrics for a satellite communication system are:

- **Average data-rate**: The average data-rate represents the expected data-rate that would be achieved in a gateway-satellite link. This value depends on the operation conditions. In this paper we report the average data-rate under *availability threshold* conditions ($Z_{99.5\%}$) and under *typical operation* conditions ($Z_{95\%}$).
- **Coverage**: The coverage metric indicates what percentage of the area targeted for service is served while satisfying the data-rate requirements. Again, we report the coverage under *availability threshold* conditions and under *typical operation* conditions, $\texttt{cov}_{99.5\%}$ and $\texttt{cov}_{95\%}$ respectively.

Statistical Formulation

Given a region of interest where service is to be provided, we are interested in determining the data-rate, coverage and availability. In other words, for any orbital position where a satellite covers the region of interest, we need to estimate the performance of the system taking into account atmospheric conditions and the fact that multiple ground stations might be visible by the satellite simultaneously. Since atmospheric attenuation is a stochastic process by nature, we adopt a statistical formulation to determine the data-rate and use it as a basis to compute the coverage and availability metrics.

Let N_{GS} be the number of ground stations in a particular ground segment architecture, and N be the number of ground stations that a satellite can access simultaneously. Let $X_i(p)$ be a random variable that describes the data-rate between a satellite located in orbital position p and the i-th ground station. This data-rate is a function of the atmospheric attenuation (also a random variable), which for high frequencies, can be as high as several tenths of dBs. Note that the relation between the data-rate and the atmospheric attenuation value is deterministic (given by the link budget equation), and therefore having the probability distribution function of the atmospheric attenuation allows us to compute the probability distribution function for the data-rate ($X_i(p)$).

Since for a particular orbital position there might be multiple ground stations in line-of-sight, we define the set of random variables that describe the data-rates achievable for each of the ground stations in the line-of-sight as:

$$\mathcal{X}(p) = \{X_i(p), ..., X_j(p)\} \tag{2}$$

In particular, $|\mathcal{X}(p)|$ is the number of ground stations in line-of-sight from orbital position p, and we refer to it as V.

Let $Y(p) = \{Y_{(1)}(p), Y_{(2)}(p), ..., Y_{(N)}(p), ..., Y_{(V)}(p)\}$ be the order statistics of a statistical sample of $\mathcal{X}(p)$, defined as the sample values placed in ascending order. In other words, the order statistics are random variables that satisfy:

$$Y_{(1)}(p) < Y_{(2)}(p) < ... < Y_{(N)}(p) < ... < Y_{(V)(p)} \tag{3}$$

such that $Y_{(1)}$ is the smallest random value of $\mathcal{X}(p)$, and $Y_{(V)}$ is the largest value:

$$Y_{(1)} = \min\{X_i(p), ..., X_j(p)\} \tag{4}$$

$$Y_{(V)} = \max\{X_i(p), ..., X_j(p)\} \tag{5}$$

Assuming that a satellite has the capability of always using the N ground stations (out of the M ground stations within the line-of-sight of the satellite) that offer the highest data-rate, the aggregated data-rate is given by

$$Z(p) = Y_{(V-N+1)} + ...Y_{(V-1)} + Y_{(V)} = \sum_{i=V-N+1}^{V} Y_{(i)} \tag{6}$$

Since each of the elements of the statistical sample comes from a different and independent statistical population (each of the random variables in $\mathcal{X}(p)$ have a different probability distribution), the *joint* probability distribution can be obtained analytically using the Bapat-Beg theorem [21]. Computing joint statistics analytically is possible because we can obtain the *marginal* distributions for each $X_i(p)$. Unfortunately, computing the analytical expression for the *joint* probability distribution involves computing an exponential number of permanent matrices, which has been shown to be computationally intractable [22].

Instead, we use Monte Carlo methods to compute the cumulative distribution function (CDF) of $Z(p)$. The simplest implementation uses direct Monte Carlo sampling to generate samples for the random variables in $\mathcal{X}(p)$ using their marginal CDF. Then, we sort the random samples and add the N largest ones to obtain a sample of $Z(p)$. The CDF of $Z(p)$ can be estimated experimentally by drawing M different samples. By doing a Monte Carlo of Monte Carlos we can estimate the error in the CDF. For example, for $N_{GS} \leq 5$ and $M = 10^5$, the error is $< 3\%$. The number of samples required to achieve a certain error can be further reduced if more advanced methods such as importance sampling are used.

Finally, note that there is an explicit dependence on the orbital position of the satellite in calculating the CDF of the aggregated data-rate ($Z(p)$), as the atmospheric attenuation is a function of the elevation angle between the satellite and the ground station. Therefore, for each orbital position one needs to compute a value of $Z(p)$ by sampling the corresponding values of the random variables in $\mathcal{X}(p)$, which can make this process computationally very intensive.

To reduce the computational burden when estimating the CDF of $Z(p)$ we use several numerical techniques which include smart discretization of the orbital positions, interpolation methods and memoisation of partial results. First, we grid the orbital sphere (the locus of all possible orbital positions a satellite might occupy) with a resolution of 0.25°x 0.25°, and we only compute the values of $Z(p)$ at these points. For each grid-point we determine which ground stations are within LoS (i.e., we compute $\mathcal{X}(p)$). Let $\mathcal{R}$ (a region) be the set of points p that have the same set of ground stations within LoS. When the number of points in $\mathcal{R}$ is small (less than 200), the CDF of $Z(p)$ is computed directly for each point, whereas when the number of points is large, we evaluate $Z(p)$ using a reduced set of points and use interpolation to compute $Z(p)$ for the rest of the points. Finally, every time that we compute the CDF of $Z(p)$ for a particular orbital position, the CDF is stored in a data base, together with the orbital position value and the list of

ground station within line-of-sight. In other words, we store key-value pairs of the form $(p, \mathcal{X}(p)) = Z(p)$. If another architecture shares the same set of ground stations within LoS from p, the CDF of $Z(p)$ is retrieved from the database without need for further computation.

3. MODELS DESCRIPTION

Overview

This section is devoted to describe the different models used to estimate the performance of a ground segment design for our reference constellation. The three most important components of our model are the *link budget model*, the *atmospheric attenuation model*, and the *demand model*. The details of each of these are introduced in the next three subsections.

To determine the best set of ground stations, we use a genetic optimization algorithm that exploits the independence of geographical distant landmasses to determine the optimal design for the ground segment. This algorithm is described in the last subsection.

Link budget model

A key component of our model is the link budget module, which computes the data-rate ($X_i(p)$) when the i-th ground station communicates with a satellite in orbital position p. Our implementation of the link budget module is parametric, and designed to allow for fast computation of the optimal modulation-coding (MODCOD) schemes for each ground station and operation conditions. This section describes the different parameters employed as inputs for the link budget for each of the EHF-bands.

We assume the use of modulation-coding schemes defined in the standards DVB-S2 [23] and DVB-S2X [24], which correspond to the second generation standard developed by the Digital Video Broadcast Project in 2003 and 2014 respectively. DVB-S2 is a standard that defines the framing structure, channel coding and modulation systems for broadcasting, interactive services, and broadband services for space-based communications. As part of the standard, a set of more than 60 MODCODs are provided, with modulations ranging from BPSK to 256-APSK, and with coding rates ranging from 1/4 to 9/10. In our link budgets, we assume a roll-off factor of 0.2 is used.

To ensure linearity and avoid distortion in the power amplifiers, we assume that the power amplifiers operate with an output back-off (OBO) equal to the peak-to-average power ratio of the MODCOD (given as the ratio between the 99.9 % percentile power and the average power). Note that in a real scenario, where all the components of the RF chain are known, one could optimize the OBO by simulating the channel and the RF chains in transmission and reception, and use pre-distortion techniques to push the PA closer to saturation.

In addition to these parameters, the link budget takes as input parameters the diameter, efficiencies, and noise temperature of the transmitter and receiver antennas, the losses in the transmitter and receiver RF chains, and the interference values from adjacent channels (CACI), satellites (CASI) and inter-modulation products (C3IM). Table 2 contains the values of these parameters for the Ka-band, Q/V-band, E-band scenarios. Note the differences in the available bandwidth, the efficiency of the antennas, the noise factor of the low noise block (LNB) downconverter and the interference level of the third order intermodulation products.

Table 2: **Link budget input parameters for the uplink feeder link**

	E-band	Q/V-band	Ka-band	Units
Frequency	83.5	50	29	[GHz]
Bandwidth	5	4	2.1	[GHz]
Roll off	0.2	0.2	0.2	[0-1]
Tx parameters				
Tx Diameter	2.4	2.4	2.4	[m]
Tx Power	100	100	100	[W]
Tx Efficiency	0.6	0.65	0.65	[0-1]
Pointing loss	0.25	0.25	0.25	[dB]
Waveguide loss	2	2	2	[dB]
Polarizer loss	0.5	0.5	0.5	[dB]
Impl. loss	0.25	0.25	0.25	[dB]
Rx parameters				
Rx Diameter	0.5	0.5	0.5	[m]
Rx Temp.	350	330	320	[K]
Rx Efficiency	0.6	0.65	0.65	[0-1]
Waveguide loss	0.1	0.1	0.1	[dB]
Pointing loss	0.25	0.25	0.25	[dB]
Feed loss	2	2	2	[dB]
Splitter loss	0.5	0.5	0.5	[dB]
Additional loss	0.5	0.5	0.5	[dB]
LNB F	4	3	2	[-]
LNB Gain	40	40	40	[dB]
LNB VSWR	1.2	1.2	1.2	[-]
Interference parameters				
CACI	25	25	25	[dB]
CASI	35	35	35	[dB]
CXPI	40	40	40	[dB]
C3IM	25	30	35	[dB]

Table 3: **Link budget for the different bands for an availability of 95 %**

Name	Ka-band	Q/V-band	E-band	Units
Elev. angle	50	50	50	[deg]
EIRP	62.81	67.54	71.64	[dBW]
Rx. Gain	41.7631	46.1469	50.6012	[dBi]
Distance	1487.42	1487.42	1487.42	[km]
FSPL	185.14	189.88	194.33	[dB]
Availability	95	95	95	[%]
Atm. Loss (tot)	1.32	4.3	5.35	[dB]
MODCOD	256APSK 32/45	256APSK L29/45	64APSK 5/6	[-]
MODCOD Γ	5.59	5.07	4.93	[bps/Hz]
MODCOD Eb/N0	11.91	10.73	10.41	[dB]
Sys. T	387.05	562.41	732.33	[K]
Rx C/N0	24.22	21.2	22.14	[dB]
Rx/(N + I)	21.1475	19.1472	18.9113	[dB]
Eb/(N0 + I)	14.46	12.89	12.77	[dB]
Link Margin	2.56	2.17	2.36	[dB]
Real Γ	4.66	4.22	4.11	[bps/Hz]
Data rate	9788.03	16885.6	20557.1	[Mbps]

Table 3 contains a summary of the link budget results for the three bands for an availability of 95 %, whereas Table 4 contains the results for an availability of 99.5 % (rows identical to the ones in Table 3 were skipped). The target

Table 4: **Link budget for the different bands for an availability of 99.5 %**

Name	Ka-band	Q/V-band	E-band	Units
Availability	99.5	99.5	99.5	[%]
Atm. Loss (tot)	4.16	10.91	16.39	[dB]
MODCOD	256APSK L29/45	32APSK 32/45	16APSK 23/36	[-]
MODCOD Γ	5.07	3.51	2.52	[bps/Hz]
MODCOD Eb/N0	10.73	7.09	5.15	[dB]
Sys. T	450.37	596.91	754.99	[K]
Rx C/N0	20.72	14.33	10.97	[dB]
Rx/(N + I)	19.0745	13.8252	10.6163	[dB]
Eb/(N0 + I)	12.82	9.16	7.39	[dB]
Link Margin	2.09	2.08	2.24	[dB]
Real Γ	4.22	2.93	2.1	[bps/Hz]
Data rate	8864.96	11700.6	10519.7	[Mbps]

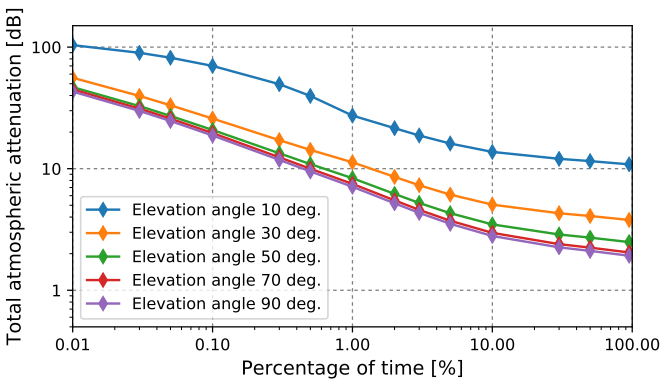

Figure 2: **Atmospheric attenuation for a ground stations located in Los Angeles for different elevation angles.**

link margin for all the scenarios is 2 dB.

Atmospheric Attenuation model

Atmospheric attenuation is the main external factor that affects the performance of a communications link. At EHF band frequencies, its effects cause link outages for non-negligible periods of time, as several tenths of dBs of attenuation may be introduced. In addition to the use of adaptive coding and modulation strategies, site diversity needs to be used to mitigate the effects of atmospheric attenuation. A satellite should have several ground stations within line-of-sight so that if the weather conditions at one particular site cause a link outage, data can still be transmitted through other ground stations.

The atmospheric attenuation for each frequency band is computed using the guidelines provided in recommendation ITU-P R.618-12 [20], which considers gaseous, clouds and fog attenuation, as well as tropospheric scintillation and rain impairments. In particular, recommendations ITU-R P.676-10 and ITU-R P.840-6 are used to compute the gaseous and clouds attenuations respectively, while the maps in recommendations ITU-R P.837-5, ITU-R P.838-3, and ITU-R P.839-4 are used to estimate the rainfall-rate, rain specific attenuation, and rain height respectively.

The method described in ITU-P R.618-12 to compute rain attenuation is valid only for percentages of time smaller than 5%. In order to overcome this limitation, we assume that the rain attenuation is 0 for percentages of time larger than the rain probability (P_0, which is computed using the method described in ITU-R P.837-5) and that the transition from the rain attenuation value at 5% to P_0 % is linear.

For each ground station, we compute the total atmospheric attenuation at different percentages of time ($\{25, 50, 75, 90, 95, 97, 99, 99.5, 99.7\}$ %), and for different elevation angle values ($\{10, 30, 50, 70, 90\}$ degrees), creating a set of CDF curves for the total atmospheric attenuation. Figure 2 shows the CDFs for different elevation angles for a ground station located in Los Angeles.

Finally, whenever present, rain attenuation is the biggest contributor to atmospheric attenuation. In this aspect, an important comment needs to be added. The rain attenuation model for slant paths in recommendation ITU-P R.618-12 is only recommended for frequencies below 55 GHz, as no measurement of atmospheric effects at higher bands were used to create the model (in fact, no measures of atmospheric attenuation in higher frequency bands exist). This issue is also true for other rain attenuation computation techniques described in recommendation ITU-P R.618-12, such as the frequency-scaling methods. Hence, by using the rain attenuation model outside of the recommended area, we might be incurring errors. This limitation has been widely recognized in the literature [13], but pending further experimental data on space-to-Earth links in W-band, we will have to contend with the best-available models.

Demand model

The demand model determines the orbital positions that satellite needs to be to cover a high enough number of users. For a given orbital altitude, we generate a gridded map (of resolution 0.25°x 0.25°) that determines the number of people covered by the beams of a satellite located in a particular orbital position. As mentioned in Section 3, we assume a minimum elevation angle of 45°for a user to be within line-of-sight of the satellite.

To generate this demand map, we use the *Gridded Population of the World (GPW) v4* dataset, which uses population census data to estimate and predict the population counts for the year 2020 over a 30-arc-second resolution grid [25]. Figure 3 shows the number of users within line-of-sight for the reference constellation (at the orbital altitude of 1,200 km). The regions with higher number of people are displayed in bright tone, whereas the regions with lower demand are displayed in darker tones.

Note that our demand model focuses on serving end users and serving as back-haul infrastructure to expand existing networks, instead of satisfying the demand of other satellite communication markets such as in-flight connectivity, marine connectivity, off-shore platform connectivity, or military connectivity. This decision was consciously taken as most of the current LEO-constellation proposals emphasize offering global bandwidth addressed towards end-users, as opposed to the aforementioned markets. [26]

Ground station selection optimization algorithm

In Section 2 we defined 3 different metrics that characterized the performance of the system. However, conducting MDO with all these metrics simultaneously is a complex problem, given the multiple trade-offs present. A common solution to simplify the optimization process involves combining all the relevant metrics in a single measure. In that sense, we define

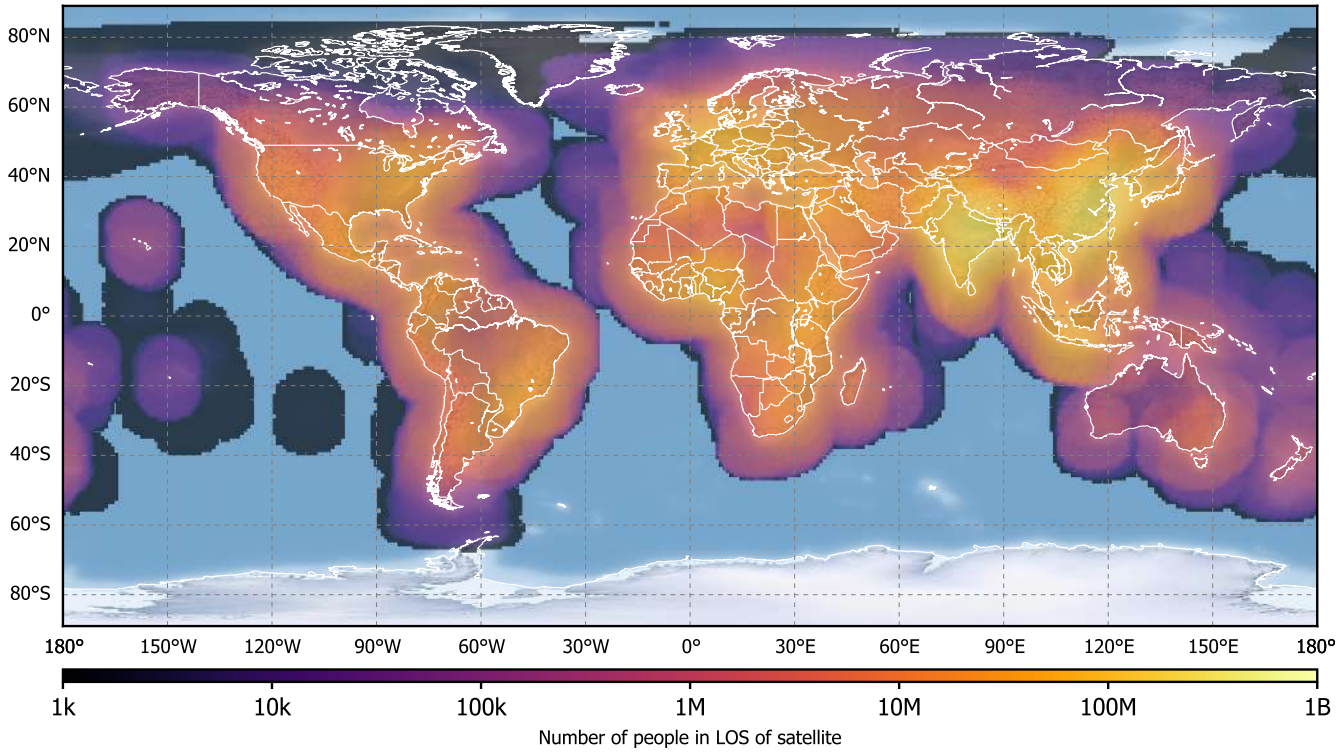

Figure 3: **Demand map for an orbital altitude of 1,200 km. The number of users within line-of-sight (elevation angle higher than 45 degrees).**

as our performance objective function

$$O = \frac{1}{2}\text{COV}_{95\%}\sum_{p\in D} Z_{95}(p)\cdot\log_{10}(f_{pop}(p)) + \frac{1}{2}\text{COV}_{99.5\%}\sum_{p\in D} Z_{99.5}(p)\cdot\log_{10}(f_{pop}(p)) \quad (7)$$

where p is a particular orbital position, D is the region in which there is some given demand, $Z_x(p)$ is the achievable data-rate at orbital position p for at least x % of the time, and $f_{pop}(\cdot)$ is a function that determines the number of people within line-of-sight of orbital position p and is used as a weighting function.

This simplifies the optimization problem at hand to maximizing the objective function in Eq. 7, while minimizing the number of ground stations required. Mathematically, this is a down-selecting problem, where we need to pick the N ground stations that offer the best performance. Given that there are 77 potential ground stations, the number of potential ground segment configurations is $2^{77} \sim 1.5\cdot 10^{23}$, which makes impossible a full numeration and evaluation of the search space. Therefore the use of optimization algorithms is called for.

Within the literature, genetic algorithms have been used to solve downselecting problems many times. In particular, we employ the Non-dominated Sorting Genetic Algorithm-II (NSGA-II) [27], an efficient multi-objective genetic algorithm, which operates as follows:

1. Generate a random population of N_{pop} architectures (populated using random subsets of ground stations)
2. Evaluate the value of the objective function O (Eq. 7) for each of them.
3. Select N/2 architectures that are the "parents" on the next generation population, attending to the following criteria [27]:
   - Architectures with lower Pareto ranking are selected first.
   - Among architectures with similar Pareto ranking, those with lower crowding distance are selected first.
4. Apply the *crossover* genetic operator over the N/2 parent-architectures. The crossover operator takes as inputs two parents and produces two offspring. Every ground station present in each parent is assigned to one of their offspring with equal probability (i.e., we use uniform crossover [28] over the ground stations on each parent). In total, N/2 offspring are produced from the N/2 parents
5. Apply the *mutation* genetic operator over the N/2 parent-architectures and the N/2 parent-architectures. Mutation removes a ground station from an architecture with probability p_{remove}, and adds a new ground station with probability p_{add}. The mutation operator is applied with probability p_{mut}.
6. Repeat steps 2-5 until a termination criterion (i.e. maximum number of generations G_{max} evaluated, no new architectures in the Pareto Front) is met.

Furthermore, we exploit the geographical structure of the problem to speed up the convergence of the optimization algorithm. Given that the selection of ground stations in one region has a small impact on which ground station are selected in another region, we divide the optimization in two phases. First, in phase A, we determine the optimal ground segment architectures for each of the 6 regions considered (see Table 8) using the NSGA-II algorithm described above

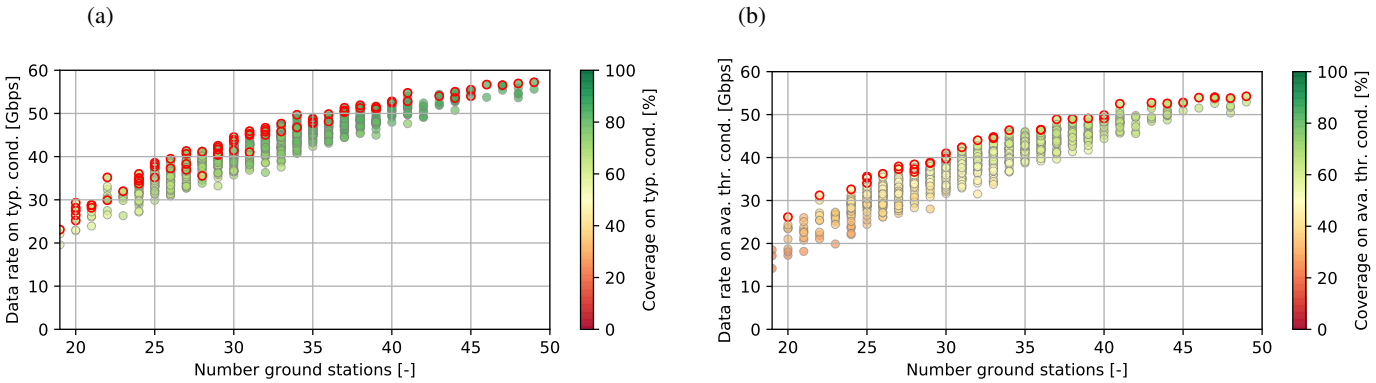

Figure 4: **Tradespace results for the E-band feeder links scenario for typical operation conditions (a) and availability threshold conditions (b). Each circle represents a ground segment architecture. Architectures in the Pareto-front are marked in red.**

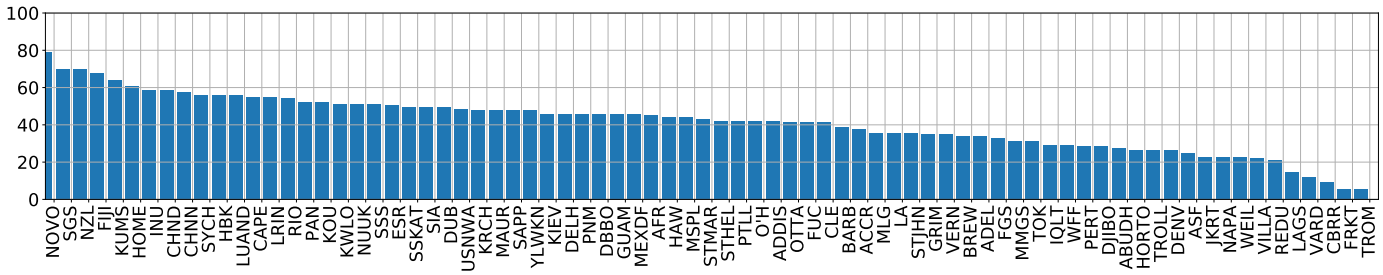

Figure 5: **Percentage of occurrence of each location in the Pareto-front architectures for the E-band scenario. The full list of ground stations can be found in Table 8**

($N_{pop} = 1000$, $G_{max} = 30$). Second, in phase B, we apply our NSGA-II algorithm globally, but instead of generating a random population (step 1), we use the Pareto-front architectures from the region based optimization in phase A as the generating components for the initial population. In other words, a ground segment architecture for phase B is generated by choosing a Pareto-optimal ground segment architectures from each of the regions in phase A. This new population serves as the initial population for the phase B NSGA-II algorithm ($N_{pop} = 500$, $G_{max} = 15$).

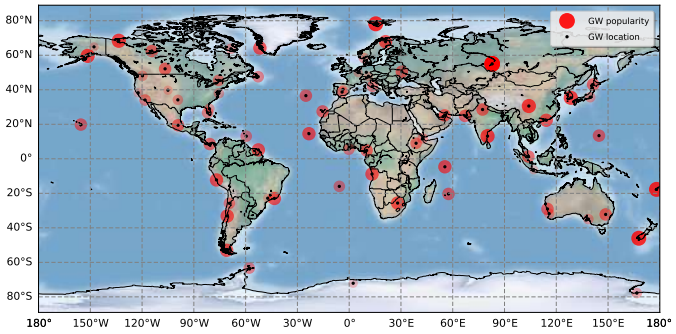

Figure 6: **World-map view of the popularity of the locations for the E-band scenario. The size and intensity of each circle is proportional to the percentage of occurrence of that location across the Pareto-front architectures.**

4. RESULTS

E-band results

Figure 4 shows the results for the E-band scenario under typical (4a) and availability threshold (4b) conditions. The horizontal axis represents the number of ground stations in the ground segment and the vertical axis the average data-rate over the demand region. The percentage of the demand region covered is represented by the color. We observe that the maximum data-rate under typical operation conditions is 57.21 Gbps, obtained when the number of ground stations is 49. Moreover, this architecture would cover 90.38% of the demand area. The data-rate and coverage under availability threshold conditions are 54.26 Gbps and 75.12% respectively. On average, the reduction in data rate of the Pareto-Front architectures between availability threshold conditions and typical conditions is 3.15 Gbps (7.77%), whereas in terms of coverage, and as for coverage the reduction is 17.82%.

Table 5 shows the average data rate Z and coverage $\texttt{cov}$ under typical and availability threshold conditions for selected Pareto-front architectures. Note that in order to achieve large coverages (> 90 % of the target region) a large number of ground stations needs to be deployed (49). And even with a large network of ground stations, 99.5% availability QoS can only be guaranteed for 75.12 % of the target region. This contrasts with current systems that achieve these performance values with much lower number of ground stations (see comparison below).

Figure 5 shows the popularity of each location within the ground segment architectures that belong to the Pareto-front, while Figure 6 shows the same information geographically on a world map. The popularity of a location is measured

Table 5: **Metrics for selected Pareto-Front architectures in the E-band scenario.**

N	$Z_{95\%}$ [Gbps]	$\text{COV}_{95\%}$ [%]	$Z_{99.5\%}$ [Gbps]	$\text{COV}_{99.5\%}$ [%]
20	29.32	59.20	26.16	39.45
25	38.57	68.07	35.25	49.16
30	44.53	75.63	40.81	54.08
35	48.66	84.00	44.81	64.17
40	52.81	84.54	49.89	68.35
45	55.50	87.47	52.83	73.29

by computing how frequently the location appears in architectures that belong to the Pareto-front. The most popular ground stations include Novosibirk, Svalbard, New Zealand, Fiji, Kumsan and Homer, whereas the least popular are Tromso, Frankfurt, Canberra and Vardo. It is interesting to note that the popular ground stations are located at either polar latitudes (e.g., Svalbard, Esrange, Inuvik, Homer), or in places where there are no other locations close by (e.g., Novosibirk, Fiji, Seychelles, New Zealand).

Q-band results

Figure 7 shows the results for the Q/V-band scenario under typical (7a) and availability threshold (7b) conditions. In this case, the maximum data-rate under typical operation conditions is 43.36 Gbps, obtained when the number of ground stations is 47. Moreover, this architecture would cover 93.27% of the demand area. The data-rate and coverage under availability threshold conditions are 40.37 Gbps and 77.50% respectively. On average, the reduction in data rate of the Pareto-Front architectures between availability threshold conditions and typical conditions is 4.13 Gbps (16.18%), whereas in terms of coverage, and as for coverage the reduction is 23.76%. Note that this greater decrease in coverage is due to the fact that Q/V-band architectures have a larger typical operations coverage compared to E-band architectures. This effect can be observed in Table 6, which contains tabulated values for selected Pareto-front architectures. Note how the $\text{COV}_{99.5\%}$ values are similar to those in Table 5 , but the values of $\text{COV}_{95\%}$ are larger in the Q/V-band scenario than in the E-band scenario.

Table 6: **Metrics for selected Pareto-Front architectures in the Q-band scenario**

N	$Z_{95\%}$ [Gbps]	$\text{COV}_{95\%}$ [%]	$Z_{99.5\%}$ [Gbps]	$\text{COV}_{99.5\%}$ [%]
20	22.58	69.13	17.09	35.14
25	28.91	76.06	23.78	49.05
30	34.06	77.69	30.93	57.47
35	38.50	86.93	35.25	67.80
40	40.29	92.11	36.28	70.84
45	43.13	91.09	40.36	74.79

The popularity of the ground stations in the Pareto Front is depicted in Figures 8 and 10. In this case, the most popular locations include Novosibirk, Kuman, Svalvard, New Zealand, Fiji and Lurin, whereas the least popular are Tromso, Redu, Lagos and Frankfurt. In view of these results, we can conclude that there are no significant differences between the most and least popular architectures in the E-band scenario and in the Q/V-band scenario.

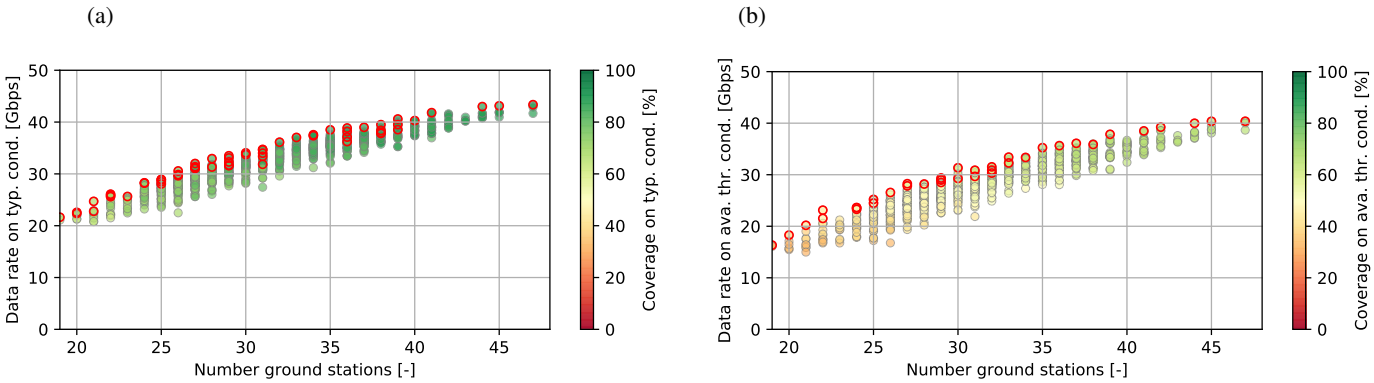

Figure 7: **Tradespace results for the Q/V-band feeder links scenario for typical operation conditions (a) and availability threshold conditions (b). Each circle represents a ground segment architecture. Architectures in the Pareto-front are marked in red.**

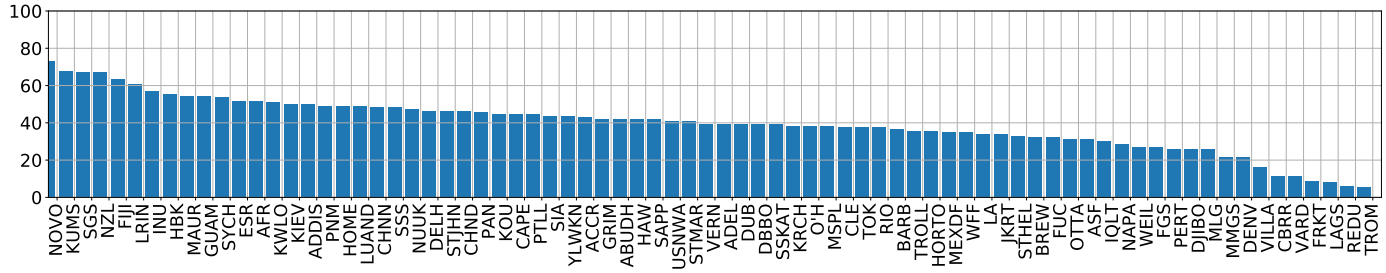

Figure 8: **Percentage of occurrence of each location in the Pareto-front architectures for the Q/V-band scenario. The full list of ground stations can be found in Table 8**.

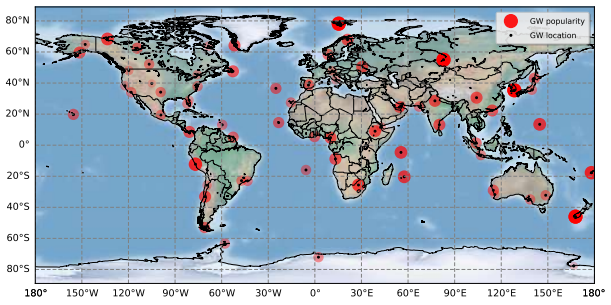

Figure 10: **World-map view of the popularity of the locations for the Q/V-band scenario. The size and intensity of each circle is proportional to the percentage of occurrence of that location across the Pareto-front architectures.**

Comparison with Ka-band and discussion

Figure 9 shows the Pareto-front architectures for the Ka, Q/V, and E-band scenarios whereas Table 7 shows a comparison of the results for 6 Pareto-front architectures with a different number of ground stations when using different frequency bands for their feeder links.

Under typical operation conditions a 45 ground stations ground segment operating in Ka-band can provide a maximum average data-rate of 29.2 Gbps, while similar systems in Q/V-band and E-band offer 43.1 Gbps and 55.5 Gbps respectively. Hence, using EHF-bands results in considerable improvements in terms of average data-rates achieved under typical operation conditions. The same is true if we consider the rates achieved when operating under threshold conditions. Ka-band systems cannot exceed a data-rate of 27 Gbps even when large ground segments are deployed, whereas the EHF-band systems easily attain these data-rates.

However, if we focus in coverage, the Ka-band system outperforms to those in EHF-bands; a much larger number of ground stations is required to maintain comparable levels of QoS. For example, the 45 ground station Ka-band system achieves a coverage under threshold conditions of 85 %, whereas a similar architecture in the EHF-band scenarios falls below 75%. Analogously, to achieve a coverage of 85 % under normal operation conditions a 30 ground stations Ka-band system would suffice, whereas 35 and 40 are needed for the Q/V-band and E-band systems respectively.

In view of these results, and specially given the coverage considerations, ground segment designs for large LEO constellations based only on EHF-systems seems infeasible, since the service is not capable of maintaining required availability levels (99.5 % of the time) at the whole coverage areas. To solve this issue, we propose two ideas that need further study to assess its feasibility:

- **Dual payload with feeder links in Ka-band and EHF-band**: In this system, both bands would be used when operating under typical conditions (giving the EHF-payload a throughput boost), whereas when operating under threshold conditions the Ka-band will ensure that wide-coverage is achieved.
- **Constellation with ISL**: As mentioned in Section 2, the use of ISL would remove the requirement of having permanent line-of-sight between a satellite and a ground station, and might result in a reduction of the number of ground stations without compromising the data-rates achieved.

(a) (b)

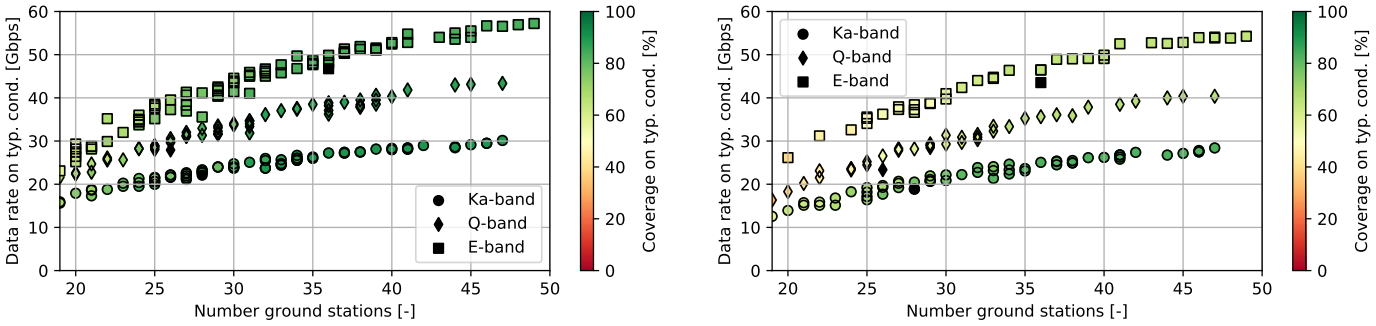

Figure 9: **Pareto Fronts for different frequency band scenarios for typical operation conditions (a) and availability threshold conditions (b).**

Table 7: **Metric comparison for Pareto-front architectures with different number of ground stations for the Ka (left), Q/V (middle) and E-band (right) scenarios.**

N	$Z_{95\%}$ [Gbps]	$\text{COV}_{95\%}$ [%]	$Z_{99.5\%}$ [Gbps]	$\text{COV}_{99.5\%}$ [%]
20	17.91	75.00	13.92	62.6
25	21.57	75.68	19.22	68.91
30	24.73	85.48	22.17	77.72
35	26.30	90.53	23.63	83.91
40	28.30	92.37	26.21	86.77
45	29.15	93.91	27.14	88.84

N	$Z_{95\%}$ [Gbps]	$\text{COV}_{95\%}$ [%]	$Z_{99.5\%}$ [Gbps]	$\text{COV}_{99.5\%}$ [%]
20	22.58	69.13	17.09	35.14
25	28.91	76.06	23.78	49.05
30	34.06	77.69	30.93	57.47
35	38.50	86.93	35.25	67.80
40	40.29	92.11	36.28	70.84
45	43.13	91.09	40.36	74.79

N	$Z_{95\%}$ [Gbps]	$\text{COV}_{95\%}$ [%]	$Z_{99.5\%}$ [Gbps]	$\text{COV}_{99.5\%}$ [%]
20	29.32	59.20	26.16	39.45
25	38.57	68.07	35.25	49.16
30	44.53	75.63	40.81	54.08
35	48.66	84.00	44.81	64.17
40	52.81	84.54	49.89	68.35
45	55.50	87.47	52.83	73.29

5. CONCLUSIONS

This paper analyzed the impact of using EHF-bands as feeder links for large constellations of communication satellite in LEO. EHF-bands have been put forth as potential solutions to increase the total capacity for future generations of these system, so as to provide truly global broadband. In particular, our analysis focused on Q/V-band and E-band, and compared these to the performance of current systems in Ka-band.

Our results show that a system in E-band with 50 ground stations can achieve an average data-rate of 55.5 Gbps over the target demand area under typical operation conditions, though this data-rate gets reduced to 52.8 Gbps under availability threshold conditions. In the Q/V-band scenario the analogous values are 43.2 and 40.4 Gbps respectively. When compared against current Ka-band systems, the data-rate that EHF-band systems can provide is considerably higher (48 % higher for Q/V-band systems and 90.4 % for E-band). However, EHF-band systems require a larger number of ground stations to provide similar coverage at comparable QoS. This observation is in contrast to what has been reported for GEO satellites, where transitioning to higher frequency bands allows for reduction of the number of gateways required.

Future Work

Several extensions of this work are possible. First, the statistical model (presented in Section 2) used to compute the aggregated data-rate could be extended, by developing a method to generate correlated samples for random variables $X_i(p)$ that correspond to closely-located ground stations. Second, when that models for atmospheric attenuation in E-band are developed using experimental data, the analysis can be run again to verify the results obtained. Finally, in a more advanced design stage, a higher fidelity link budget model can be developed, in such a way that a) the losses and interference parameters are more accurately modeled and b) all the design parameters are optimized to achieve maximum performance (for example, the power amplifier OBO).

Furthermore, from an analysis perspective, it would be interesting to study the performance of a hybrid system, where satellites carry dual Ka-band and EHF-band payloads for their feeder links. Both transponders would be used under typical operation conditions, while the Ka-band transponder would be the primary transponder under threshold conditions. Also, an analysis similar to the one conducted in this paper but with the assumption that the reference constellation has inter-satellite links might be highly beneficial. Having ISL would remove the requirement of having permanent line-of-sight between a satellite and a ground station, and might result in a reduction of the number of ground stations without compromising the data-rates achieved.

ACKNOWLEDGMENTS

The authors would like to thank the *Fundación Obra Social de La Caixa* for partially funding this project.

Table 8: **List of candidate ground stations.**

ID	Name	Code	Latitude	Longitude	Country	Organization	Region
1	Alaska Satellite Facility	ASF	64.86	-147.85	USA	NEN (NASA)	N. America
2	Clewiston	CLE	26.73	-82.03	USA	SSC	N. America
3	Esrange	ESR	67.88	21.07	Sweden	SSC	Europe
4	Florida Ground Station	FGS	29.00	-81.00	USA	NEN (NASA)	N. America
5	Fucino	FUC	42.00	13.55	Italy	SSC	Europe
6	Hartebeesthoek	HBK	-25.64	28.08	South Africa	SSC	Africa
7	Inuvik	INU	68.40	-133.50	Canada	SSC	N. America
8	McMurdo Ground Station	MMGS	-77.81	166.69	Antartica	NEN (NASA)	Oceania
9	O'Higgins	O'H	-63.32	-57.90	Antartica	SSC	S. America
10	Punta Arenas	PAN	-53.00	-71.00	Argentina	SSC	S. America
11	Santiago Satellite Station	SSS	-33.13	-70.67	Chile	SSC	S. America
12	Svalbard Ground Station	SGS	78.22	15.39	Norway	NEN (NASA)	Europe
13	USN Western Australia	USNWA	-29.05	114.90	Australia	SSC	Oceania
14	Wallops Flight Facility Ground Stations	WFF	37.94	-75.49	USA	NEN (NASA)	N. America
15	Weilheim	WEIL	47.84	11.14	Germany	SSC	Europe
16	Hawaii	HAW	19.82	-155.47	USA	KSAT	N. America
17	Tokyo	TOK	35.69	139.69	Japan	KSAT	Asia
18	Singapore	SIA	1.35	103.82	Singapore	KSAT	Asia
19	Trollsat	TROLL	-72.10	2.32	Antartica	KSAT	Africa
20	Vardo	VARD	70.37	31.10	Norway	KSAT	Europe
21	Tromso	TROM	69.65	18.96	Norway	KSAT	Europe
22	Grimstad	GRIM	58.34	8.59	Norway	KSAT	Europe
23	Puertollano	PTLL	38.69	-4.11	Spain	KSAT	Europe
24	Dubai	DUB	25.20	55.27	UAE	KSAT	Asia
25	Mauritius	MAUR	-20.35	57.55	Mauritius	KSAT	Africa
26	Panama	PNM	8.54	-80.78	Panama	KSAT	S. America
27	Central Africa	AFR	4.84	10.10	Central Africa	KSAT	Africa
28	New Zeland	NZL	-46.02	167.81	New Zeland	KSAT	Oceania
29	Kourou	KOU	5.16	-52.65	French Guiana	ESA	S. America
30	Redu	REDU	50.00	5.16	Belgium	ESA	Europe
31	Cebreros	CBRR	40.46	4.46	Spain	ESA	Europe
32	Villafranca	VILLA	40.26	-3.57	Spain	ESA	Europe
33	Maspalomas	MSPL	27.45	-15.38	Spain	ESA	Europe
34	Santa Maria	STMAR	36.59	-25.08	Portugal	ESA	Europe
35	Malargue	MLG	-25.78	-69.40	Argentina	ESA	S. America
36	Frankfurt	FRKT	50.12	9.92	Germany	ESA	Europe
37	Perth	PERT	-31.80	115.89	Australia	ESA	Oceania
38	Delhi	DELH	28.55	77.29	India	Viasat	Asia
39	Chennai	CHNN	13.13	80.17	India	Viasat	Asia
40	Chengdu	CHND	30.58	104.11	China	Other	Asia
41	Jakarta	JKRT	-6.34	106.86	Indonesia	Indosat	Asia
42	Novosibirk	NOVO	55.02	82.84	Russia	Other	Asia
43	Rio de Janeiro	RIO	-22.98	-43.35	Brazil	SES	S. America
44	Addis Ababa	ADDIS	9.01	38.76	Ethiopia	SES	Africa
45	New Caledonia	NEWC	-22.26	166.40	New Caledonia	Intelsat	Oceania
46	Guam	GUAM	13.42	144.75	USA	NEN (NASA)	Asia
47	Saint Helena	STHEL	-15.97	-5.71	Saint Helena	Other	Africa
48	Sychelles	SYCH	-4.63	55.45	Sychelles	Laban	Africa
49	Luanda	LUAND	-8.84	13.23	Angola	Other	Africa
50	Barbados	BARB	13.10	-59.63	Barbados	Other	S. America
51	Alaska	HOME	59.65	-151.54	USA	NEN (NASA)	N. America
52	Nuuk	NUUK	64.18	-51.74	Greenland	Other	N. America
53	Sapporo	SAPP	43.06	141.34	Japan	JAXA	Asia
54	Adelaide	ADEL	-34.93	138.60	Australia	SES	Oceania
55	Accra	ACCR	5.56	-0.20	Gahna	SES	Africa
56	Lagos	LAGS	6.52	3.38	Nigeria	SES	Africa
57	Lurin	LRIN	-12.25	-76.88	Peru	SES	S. America
58	Hortolandia	HORTO	-22.85	-47.21	Brazil	SES	S. America
59	Dijbouti	DJIBO	11.83	42.59		SES	Africa
60	Abu Dhabi	ABUDH	24.45	54.38	UAE	SES	Asia
61	Kowoloon	KWLO	22.32	114.18	Hong Kong	SES	Asia
62	Brewster	BREW	48.09	-119.78	USA	SES	N. America
63	Los Angeles	LA	34.05	-118.24	USA	SES	N. America
64	Vernon	VERN	34.15	-99.27	USA	SES	N. America
65	Karachi	KRCH	24.86	67.10	Pakistan	SES	Asia
66	Kiev	KIEV	50.45	30.52	Ukraine	SES	Europe
67	Dubbo	DBBO	-32.23	148.63	Australia	SES	Oceania
68	Denver	DENV	39.74	-104.99	USA	Intelsat	N. America
69	Kumsan	KUMS	35.36	128.41	South Korea	Intelsat	Asia
70	Napa	NAPA	38.25	-122.28	USA	Intelsat	N. America
71	Ottawa	OTTA	45.42	-75.70	Canada	Telesat	N. America
72	Yellowknife	YLWKN	62.45	-114.37	Canada	Telesat	N. America
73	St. John's	STJHN	47.56	-52.71	Canada	Telesat	N. America
74	Iqaluit	IQLT	63.75	-68.52	Canada	Telesat	N. America
75	Saskatoon	SSKAT	52.13	-106.67	Canada	Telesat	N. America
76	Mexico DF	MEXDF	19.43	-99.13	Mexico	Eutelsat	N. America
77	Cape Verde	CAPE	14.55	-23.31	Cape Verde	Other	Africa

REFERENCES

[1] WorldVu Satellites Limited, "OneWeb Ka-band NGSO constellation FCC filing SAT-LOI-20160428-00041," Available at http://licensing.fcc.gov/myibfs/forwardtopublictabaction.do?file_number=SATLOI2016042800041 (2017/09/12).

[2] Space Exploration Holdings, LLC, "SpaceX Ka-band NGSO constellation FCC filing SAT-LOA-20161115-00118," Available at http://licensing.fcc.gov/myibfs/forwardtopublictabaction.do?file_number=SATLOA2016111500118 (2017/09/12).

[3] The Boeing Company, "Boeing V-band NGSO constellation FCC filing SAT-LOA-20160622-00058," Available at http://licensing.fcc.gov/myibfs/forwardtopublictabaction.do?file_number=SATLOA2016062200058 (2017/09/12).

[4] Telesat Canada, "Telesat Ka-band NGSO constellation FCC filing SAT-PDR-20161115-00108," Available at http://licensing.fcc.gov/myibfs/forwardtopublictabaction.do?file_number=SATPDR2016111500108 (2017/09/12).

[5] U. J. Lewark, J. Antes, J. Walheim, J. Timmermann, T. Zwick, and I. Kallfass, "Link budget analysis for future e-band gigabit satellite communication links (71–76 and 81–84 ghz)," *CEAS Space Journal*, vol. 4, no. 1, pp. 41–46, Jun 2013. [Online]. Available: https://doi.org/10.1007/s12567-013-0030-0

[6] O. Vidal, G. Verelst, J. Lacan, E. Alberty, J. Radzik, and M. Bousquet, "Next generation high throughput satellite system," in *Satellite Telecommunications (ESTEL), 2012 IEEE First AESS European Conference on*. IEEE, 2012, pp. 1–7.

[7] WorldVu Satellites Limited, "OneWeb V-band NGSO constellation FCC filing SAT-LOI-20170301-00031," Available at http://licensing.fcc.gov/myibfs/forwardtopublictabaction.do?file_number=SATLOI2017030100031 (2017/09/12).

[8] Space Exploration Holdings, LLC, "SpaceX V-band NGSO constellation FCC filing SAT-LOA-20170301-00027."

[9] R. Polonio and C. Riva, "Italsat propagation experiment at 18.7, 39.6 and 49.5 ghz at spino d'adda: three years of cpa statistics," *IEEE transactions on antennas and propagation*, vol. 46, no. 5, pp. 631–635, 1998.

[10] M. Mauri, A. Paraboni, and A. Pawlina, "The olympus and italsat propagation programs of the italian space agency: An overview of the first experimental results in the 12 to 50 ghz frequency bands," in *Satellite Communications-ECSC-3, 1993., 3rd European Conference on*. IET, 1993, pp. 263–268.

[11] J. Fawcette, "Milstar: Hotline in the sky." *HIGH TECHNOL.*, vol. 3, no. 11, pp. 62–63, 1983.

[12] G. Elfers and S. B. Miller, "Future u. s. military satellite communication systems," *Crosslink*, vol. 3, no. 1, pp. 46–52, 2001.

[13] E. Cianca, T. Rossi, A. Yahalom, Y. Pinhasi, J. Farserotu, and C. Sacchi, "Ehf for satellite communications: The new broadband frontier," *Proceedings of the IEEE*, vol. 99, no. 11, pp. 1858–1881, 2011.

[14] A. Jebril, M. Lucente, E. Re, T. Rossi, M. Ruggieri, C. Sacchi, and V. Dainelli, "Perspectives of w-band for space communications," in *2007 IEEE Aerospace Conference*, March 2007, pp. 1–12.

[15] T. Rossi, F. Maggio, M. D. Sanctis, M. Ruggieri, S. Falzini, and M. Tosti, "System analysis of smart gateways techniques applied to q/v-band high throughput satellites," in *2014 IEEE Aerospace Conference*, March 2014, pp. 1–10.

[16] T. Rossi, M. De Sanctis, D. Di Mattia, and M. Ruggieri, "Performance analysis and optimization of site diversity techniques for ehf satellite links," in *Aerospace Conference, 2011 IEEE*. IEEE, 2011, pp. 1–11.

[17] I. del Portillo and M. Sanchez and B. Cameron and E. Crawley, "Optimal location of optical ground stations to serve leo spacecraft," in *2017 IEEE Aerospace Conference*, March 2017, pp. 1–16.

[18] I. del Portillo and M. Sanchez and B. Cameron and E. Crawley, "Architecting the ground segment of an optical space communication network," in *2016 IEEE Aerospace Conference*, March 2016, pp. 1–13.

[19] I. T. Unit, "Space Network List database," Available at http://www.itu.int/en/ITU-R/space/snl/ (2017/09/04).

[20] P. Series, "Propagation data and prediction methods required for the design of earth-space telecommunication systems," *Recommendation ITU-R*, pp. 618–12, 2015.

[21] R. Bapat and M. Beg, "Order statistics for nonidentically distributed variables and permanents," *Sankhyā: The Indian Journal of Statistics, Series A*, pp. 79–93, 1989.

[22] D. H. Glueck, A. Karimpour-Fard, J. Mandel, L. Hunter, and K. E. Muller, "Fast computation by block permanents of cumulative distribution functions of order statistics from several populations," *Communications in Statistics-Theory and Methods*, vol. 37, no. 18, pp. 2815–2824, 2008.

[23] Digital Video Broadcasting (DVB), "Second generation framing structure, channel coding and modulation systems for broadcasting, interactive services, news gathering," DVB-S2 draft document DVBS2-83, Tech. Rep., 6 2003.

[24] ——, "Second generation framing structure, channel coding and modulation systems for broadcasting, interactive services, news gathering and other broadband satellite applications; part2: Dvb-se extensions (dvb-s2x)," DVB-S2X draft document DVBS2-83, Tech. Rep., 6 2014.

[25] C. CIESIN, "Gridded population of the world version 4 (gpwv4): population density grids," *Palisades, NY: Socioeconomic Data and Applications Center (SEDAC), Columbia University*, 2005.

[26] W. A. Hanson, "In their own words: Oneweb's internet constellation as described in their fcc form 312 application," *New Space*, vol. 4, no. 3, pp. 153–167, 2016.

[27] K. Deb, A. Pratap, S. Agarwal, and T. Meyarivan, "A fast and elitist multiobjective genetic algorithm: NSGA-II," *Evolutionary Computation, IEEE Transactions on*, vol. 6, no. 2, pp. 182–197, 2002.

[28] G. Syswerda, "Uniform crossover in genetic algorithms," 1989.

BIOGRAPHY

Iñigo del Portillo *is a Ph.D. candidate in the department of Aeronautics and Astronautics at MIT. His research interests include system architecture for space-based networks, space optical communications systems, and small satellites communications. Iñigo received his degrees in Industrial Engineering, Electronics Engineering and Telecommunications Engineering in 2014 from Universitat Politecnica de Catalunya, Barcelona, and his M.Sc. in Aeronautics and Astronautics from MIT in 2016.*

Dr. Bruce Cameron *is a Lecturer in Engineering Systems at MIT and a consultant on platform strategies. At MIT, Dr. Cameron ran the MIT Commonality study, a 16 firm investigation of platforming returns. Dr. Cameron's current clients include Fortune 500 firms in high tech, aerospace, transportation, and consumer goods. Prior to MIT, Bruce worked as an engagement manager at a management consultancy and as a system engineer at MDA Space Systems, and has built hardware currently in orbit. Dr. Cameron received his undergraduate degree from the University of Toronto, and graduate degrees from MIT.*

Dr. Edward F. Crawley *received an Sc.D. in Aerospace Structures from MIT in 1981. His early research interests centered on structural dynamics, aeroelasticity, and the development of actively controlled and intelligent structures. Recently, Dr. Crawley's research has focused on the domain of the architecture and design of complex systems. From 1996 to 2003 he served as the Department Head of Aeronautics and Astronautics at MIT, leading the strategic realignment of the department. Dr. Crawley is a Fellow of the AIAA and the Royal Aeronautical Society (UK), and is a member of three national academies of engineering. He is the author of numerous journal publications in the AIAA Journal, the ASME Journal, the Journal of Composite Materials, and Acta Astronautica. He received the NASA Public Service Medal. Recently, Prof Crawley was one of the ten members of the presidential committee led by Norman Augustine to study the future of human spaceflight in the US.*